Journal of Environmental Sciences 159 (2026) 490–501

Contents lists available at ScienceDirect

Journal of Environmental Sciences

journal homepage: www.elsevier.com/locate/jes

JES JOURNAL OF ENVIRONMENTAL SCIENCES www.jesc.ac.cn

Research Article

Spatiotemporal characteristics of atmospheric CO_2 under the influence of different industrial emission sources using lidar remote sensing in Nanping, China

Saifen Yu[a,b,c], Daihao Yu[a], Qiuwei Xia[a,c], Yixiang Chen[a], Zhen Zhang[a,b,c,*], Haiyun Xia[a,b,d,*]

[a] School of Atmospheric Physics, Nanjing University of Information Science and Technology, Nanjing 210044, China
[b] National Center of Carbon Metrology (Fujian), Nanping 353011, China
[c] Fujian Ruitan Optoelectronic Precision Instrument Co., Ltd., Nanping 353011, China
[d] School of Earth and Space Science, University of Science and Technology of China, Heifei 230026, China

ARTICLE INFO

Keywords:
Lidar
CO_2
Wind field
Spatiotemporal variations
Carbon emission

ABSTRACT

Atmospheric CO_2 concentrations are predominantly regulated by multiple emission sources, with industrial emissions representing a critical anthropogenic driver that significantly influences temporal and spatial heterogeneity in regional CO_2 patterns. This study investigated the spatiotemporal distribution of atmospheric CO_2 in Pucheng and Nanping industrial parks, Nanping City, by conducting field experiments using two coherent differential absorption lidars from 1 August to 31 October 2024. Results showed that the spatial distributions of CO_2 emissions within a 3 km radius were mapped, and the local diffusion processes were clarified. CO_2 patterns varied differently in two industrial parks over the three-month period: Average CO_2 concentrations in non-emission areas were 422.4 ppm in Pucheng and 408.7 ppm in Nanping, with the former experiencing higher and more variable carbon emissions; Correlation analysis indicated that synthetic leather factories in Pucheng contributed more to SO_2 and NO_x levels compared to the chemical plant in Nanping; In Pucheng, CO_2 concentrations were transported from the north at ground-level wind speeds exceeding 4 m/s, while in Nanping, the concentrations dispersed gradually with increasing wind speeds; Forward trajectory simulations revealed that the peak-emission from Pucheng primarily affected southern Fujian, northeastern Jiangxi, and southern Anhui, while the peak-emission from Nanping influenced central and western Fujian and northeastern Jiangxi. Besides, emissions in both industrial parks were higher on weekdays and lower on weekends, reflecting changes in industrial activities. The study underscores the potential of lidar technology for providing detailed insights into CO_2 distribution and the interactions between emissions, wind patterns, and carbon transport.

1. Introduction

Atmospheric carbon dioxide (CO_2) is one of the most significant greenhouse gases, and its concentration is closely related to atmospheric temperature (Lüthi et al., 2008). Since the industrial revolution, human activities have become heavily dependent on the combustion of fossil fuels, leading to increased CO_2 and pollutant emissions (Gregg et al., 2008; Hofmann et al., 2009; Li et al., 2012; Friedlingstein et al., 2023; Van Oosterhout et al., 2024). Thanks to the role of CO_2 sinks such as oceans and terrestrial ecosystems, atmospheric CO_2 concentrations are rising at approximately half the rate of fossil fuel emissions (Prentice et al., 2001; Turnbull et al., 2011). During the 2011–2020 period, about 48 % of human-caused emissions accumulated in the atmosphere, 26 % were absorbed by the oceans, and 29 % were stored on land, leaving an unaccounted imbalance of 3 % (Friedlingstein et al., 2022). The portion of CO_2 from fossil fuel combustion and other emission sources that remain in the atmosphere varies from year to year due to the significant natural variability of CO_2 sinks, without a confirmed global trend (Le Quéré et al., 2009; Andres et al., 2012). Understanding the disturbance budget over time and the potential changes and trends in the natural carbon cycle is necessary for identifying peak emission periods, assessing the dispersion of pollutants, as well as understanding the response of natural sources or sinks to driving factors of climate change (Friedlingstein et al., 2023). However, the interaction between natural carbon sinks and anthropogenic emissions in high-vegetation regions remains poorly understood due to limited observational data, hindering accurate predictions of future CO_2 levels and their impact on climate change (Lobell et al., 2008).

The World Meteorological Organization's Global Atmosphere Watch Program (WMO/GAW) coordinates a global network of observations

* Corresponding authors.
E-mail addresses: 003514@nuist.edu.cn (Z. Zhang), hsia@ustc.edu.cn (H. Xia).

https://doi.org/10.1016/j.jes.2025.03.046
Received 22 December 2024; Received in revised form 12 March 2025; Accepted 26 March 2025
Available online 27 March 2025

and analyses of greenhouse gases (Fang et al., 2014). The global average surface CO_2 concentration reached 420 ppm by 2023 (Lan et al., 2024). In addition, China has set up several atmospheric background observation stations across the Country (Xia et al., 2020). The observed data shows that in 2022, the annual average CO_2 concentration recorded at Lin'an Station in Zhejiang Province was the highest with a value of 437.7 ppm, while the lowest concentration recorded at the Waliguan National Atmospheric Background Station was 419.3 ppm. The measurements of those stations are mainly based on in-situ instruments and are used for studying greenhouse gas concentrations in the atmospheric background (Xia et al., 2015; Cheng et al., 2018). However, industrial emission sources exhibit more pronounced spatiotemporal variations (Henninger and Kuttler, 2010; Zhang et al., 2024), influenced by daily operational cycles, energy demand, and diurnal fluctuations. Traditional ground-based in-situ measurement methods, while highly precise, are confined to point-specific concentration data (Lewicki et al., 2005), offering limited spatial coverage and often failing to capture broader spatial and temporal variability. In areas with complex terrain or multiple emission sources, these methods frequently overlook critical variations between measurement points, leading to an inadequate representation of overall emission patterns (Queiβer et al., 2019). In contrast, Differential Absorption Lidar (DIAL) offers high spatiotemporal resolution measurements of mesoscale CO_2 concentrations over a range of up to several kilometers (Lahyani et al., 2021; Gibert et al., 2015; Yu et al., 2021a). Additionally, coherent DIAL provides precise vertical and horizontal profiling of gas concentrations and wind simultaneously (Yu et al., 2024), making it an ideal choice for high-vegetation regions affected by varying industrial emission sources and providing deeper insights into CO_2 distribution and transport dynamics. CO_2 DIAL technology has been proven to be employed for volcanic or industrial carbon emissions monitoring from the ground-based platform (Queiβer et al., 2016; Yue et al., 2022). However, there are few long-term observations on the impact of industrial emissions on local atmospheric CO_2 levels in different areas and from different climatic regions, especially in areas with high forest coverage.

Nanping City is located in the northern part of Fujian Province and is a key forest area in southern China. It is rich in carbon sink resources with a forest coverage rate of 74.75 % (Zhao et al., 2021). Forests act as vital carbon sinks, absorbing large quantities of CO_2 from the atmosphere through photosynthesis, which helps mitigate the rise in atmospheric CO_2 levels (Pan et al., 2011). Meanwhile, three major industrial clusters have been established within the city to support economic growth and industrialization, which inevitably emit CO_2 into the atmosphere as carbon sources. Thus, in industrial parks with high forest coverage, the distribution of CO_2 concentration in the surrounding atmosphere is significantly affected by natural carbon sequestration processes and anthropogenic emissions. The region is of great value for studying the interaction between carbon sources and sinks on a regional scale to better understand the links between the various components of the carbon cycle. Based on the geographical conditions and the measurement advantages of DIAL, the objectives of this study were to: (1) compare the impact of different industrial emission sources on the spatial distribution of CO_2 concentration in areas with high carbon sink resources; (2) clarify the temporal variation characteristics of CO_2 concentration in emission and non-emission areas; (3) elucidate the relationship between CO_2 concentrations and other pollutants, as well as infer the types of emission sources; (4) investigate the influence of meteorological conditions on CO_2 concentration for different emission sources by combining wind field; (5) analyze the possible transport pathways and impact area of carbon emissions based on forward trajectory modeling. The study explored the spatiotemporal characteristics of CO_2 concentrations in regions affected by different industrial emissions, providing insights into the relationship between industrial activity and CO_2 dynamics. By examining these time-space-dependent patterns, we can better understand the role of industrial emissions in shaping the atmospheric CO_2 profile and inform more effective strategies for emission control and climate mitigation.

2. Materials and methods

2.1. Study site and instruments

When conducting atmospheric gas measurements, research shows that the observation period for ground-based surface network species should be no less than three months to avoid being affected by the data variability (Wang et al., 2022). Thus, the experiments were simultaneously conducted near two industrial parks located in the southern (Yanping District, named Nanping industrial park) and northern (Pucheng County, named Pucheng industrial park) of the three major clusters in Nanping City, China (27.99°N, 118.55°E and 26.53°N, 118.29°E) from 1 August 2024 to 31 October 2024. As shown in Fig. 1**a**, Pucheng industrial park is located along a north-south axis within mountainous terrain while Nanping industrial park is an enclosed basin. Besides, the land use data shows that the vast majority of Nanping's areas are covered by forests. The vegetation covers in two locations are dominated by warm temperate evergreen broad-leaved forests, which maintain high photosynthetic rates across all seasons. And two CO_2 DIALs have been placed in Pucheng industrial park and Nanping industrial park for remote sensing of wind fields and CO_2 concentrations (Fig. 1**b and c**).

The measurement areas were extended by conducting plan position indicator (PPI) scanning mode. Besides, Pucheng industrial park is located 3.5 km north of the County town, and the scanning range of the region mainly includes some synthetic leather factories, biomass energy, aluminum and electrical plants (Fig. 2**b**). The synthetic leather factories mainly emit CO_2 by consuming electricity from the power grid through coal-fired power generation (Chowdhury et al., 2017). In addition, there are some scattered factories located north of the DIAL, which are beyond the scanning range. Meanwhile, the DIAL at Nanping industrial park covered a large chemical plant producing silicone and biomass carbon rods. Besides, a small cement plant was located about 300 m west of the DIAL, which was not within the scanning range of the DIAL. The two industrial parks are representative of typical industrial emission sources in Nanping and are close to major urban and forest areas, allowing for a comprehensive analysis of the interaction between industrial emissions and atmospheric CO_2 concentrations.

The meteorological conditions in two industrial parks are essential for interpreting CO_2 dynamics and validating measurement accuracy. Fig. 2 shows the meteorological conditions including air temperature, relative humidity, visibility, downward solar radiation and precipitation from 1 August 2024 to 31 October 2024 in two industrial parks. Temperature and relative humidity regulate atmospheric diffusion processes, while downward solar radiation affects both atmospheric stability and plant photosynthetic activity. During the observation period, the monthly averaged temperature, relative humidity and downward solar radiation in both industrial parks exhibited similar temporal trends, which typically ranged between 20.9–29.6 °C, 72.7 %–78.9 % and 126.9–211.9 W/m^2, respectively (Fig. 2**a, b and d**). The visibility in Pucheng industrial park was lower than that in Nanping industrial park, with an average of 15.0 and 23.4 km respectively (Fig. 2**c**). Both values substantially exceeded the minimum threshold required for reliable DIAL measurements, ensuring data quality. Precipitation contributes to CO_2 removal through wet deposition. More abundant precipitation appeared in Nanping industrial park, with a maximum monthly accumulated value of 618.3 mm in August and a sub-maximum value of 470.6 mm in September. Otherwise, the monthly accumulated precipitation varied from 145.8–244.4 mm (Fig. 2**e**).

The two DIALs in Pucheng and Nanping industrial parks possess the same system parameters except for the aperture of the telescopes, which mainly affects the detection distance. The maximum detection distance of the former is 6 km while that of the latter is 3 km. For ease of comparison, the data ranges of the two DIALs in both industrial parks were set

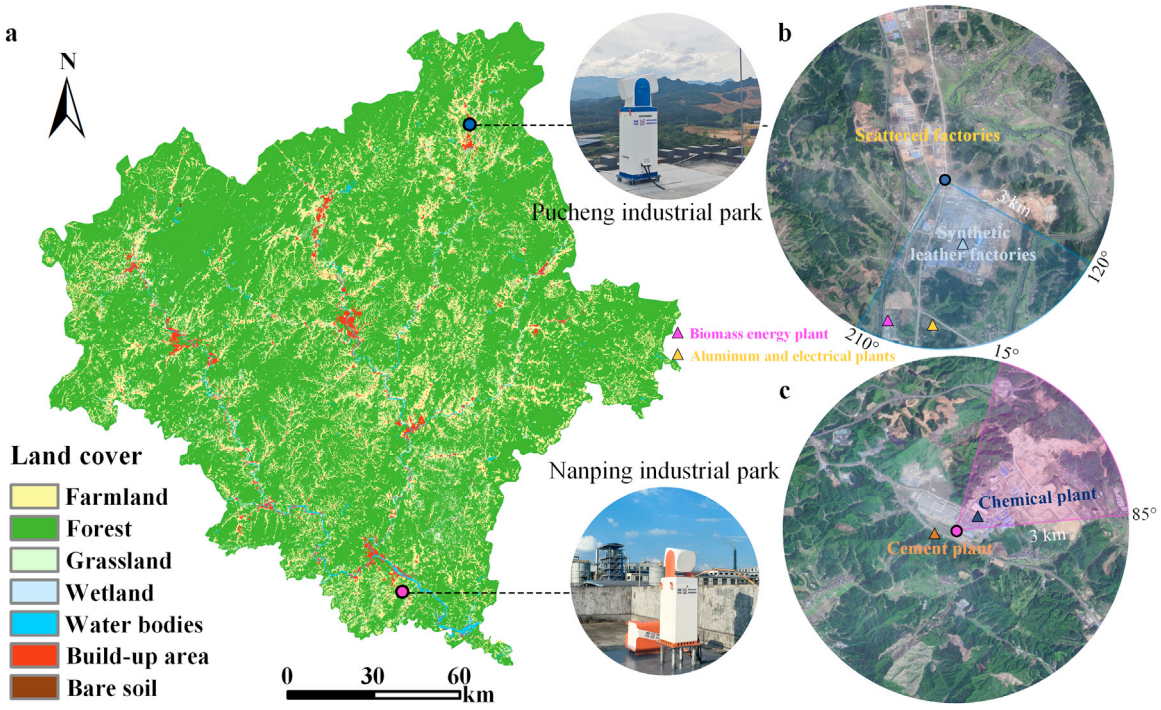

Fig. 1 – (a) Land cover in Nanping City in 2020; (b) lidar site at Pucheng industrial park; (c) lidar site at Nanping industrial park.

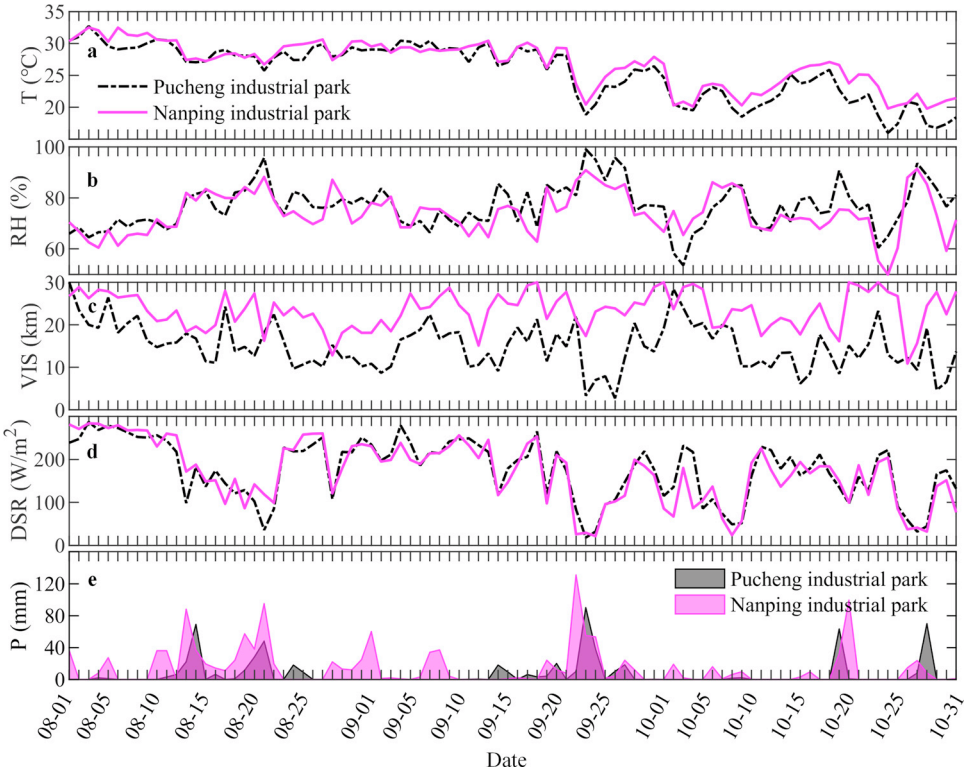

Fig. 2 – Mean daily (a) air temperature (T); (b) relative humidity (RH); (c) visibility (VIS); (d) downward solar radiation (DSR); (e) precipitation (P) from 1 August 2024 to 31 October 2024 in Pucheng and Nanping industrial parks. T, RH, VIS and P were obtained from the measurements of local meteorological stations, and DSR was from the ERA5 datasets with a horizontal resolution of 0.25° × 0.25°.

to the same of 3 km. The measurement accuracy of CO_2 was specified with a mean error of 2.05 ppm and a standard deviation of 7.18 ppm (Yu et al., 2024). Although the DIAL systems exhibit lower measurement accuracy and time resolution compared to the in-situ instruments, they provide large-range measurements of both CO_2 and wind fields from a safe distance through scanning and remote sensing. The azimuth angle of PPI scanning in Pucheng industrial park ranged from 120° to 210° and in Nanping industrial park ranged from 15° to 85°, with an azimuth step of 2°. This scanning setup covered most of the factory areas and the areas without emission sources while ensuring the operational efficiency of DIALs. Besides, in order to avoid building obstruction as much as possible, two DIALs were set with elevation angles of 1° and 9° respectively. The sampling sites were adequate to represent the pollution level of our study regions.

2.2. Methods

The carrier-to-noise ratio (CNR), CO_2 concentration and wind field data were obtained from two coherent CO_2 DIALs measurements. Coherent DIAL emitted two laser beams of different wavelengths into the atmosphere (one wavelength at the CO_2 absorption peak called on-line and the other wavelength at a position not absorbed by CO_2 called off-line). The backscatter signals presented a beat note between a local oscillator and atmospheric scatter whose frequency was related to the Doppler shift and whose amplitude was related to the power of the atmospheric scatter (Koch et al., 2004). Thus, CNR and radial wind were inverted by the Doppler shift and amplitude of backscatter signals at different positions along the emitted path, respectively. Among them, CNR represents the mean radio-frequency signal power to the mean noise power, which reflects the backscattering signal intensity from an aerosol (Yu et al., 2021b). When the DIALs perform measurements at a certain elevation angle, hard targets such as buildings or mountain terrain, as well as the heavily polluted atmosphere or even fog can cause CNR enhancement. CNR and CO_2 concentration were positively related while emitted plumes by industries within the DIALs scanning range contained CO_2. Besides, the atmospheric temperature and pressure were measured by the thermometer and barometer inserted in the DIALs, which were used to combine the lidar equation to invert the CO_2 concentration through the difference between on-line and off-line CNRs (Gibert et al., 2015). The negative values of radial wind speed indicate being away from the DIAL, while the positive values indicate pointing towards the DIAL. Additionally, based on the radial wind speed measured by lidar, the variational method was used to invert the two velocity components of wind speed in the horizontal plane, thereby obtaining two-dimensional wind field data of horizontal wind speed and horizontal wind direction (Yuan et al., 2022). The time and range resolutions of each radial measurement by DIALs were 1 min and 120 m.

The land cover map was drawn using the GlobeLand 30 dataset developed by the National Geomatics Center of China with a resolution of 30 m for the year 2020. The classification system of the GlobeLand 30 includes ten land cover types, and the overall accuracy is 83.5 % (Chen et al., 2017). In this study, seven land cover types including farmland, forest, grassland, wetland, wave body, built-up area and bare soil were comprised.

The air temperature, relative humidity, visibility, precipitation and $PM_{2.5}$ were obtained from the nearest local meteorological stations (located at 27.92°N, 118.53°E for Pucheng industrial park and 26.65°N, 118.17°E for Nanping industrial park) in proximity to the two DIALs. Those meteorological parameters were recorded at 3-hour intervals, and daily averages were calculated from the measurements to represent the overall conditions for each day.

The downward solar radiation data were obtained from the ERA5 reanalysis dataset, which offered a spatial resolution of 0.25° × 0.25° and a temporal resolution of 1-hour intervals. The ERA5 dataset was selected for its robust integration of multiple observational sources, including satellite measurements, ground-based observations, and atmospheric models, through advanced data assimilation techniques. This comprehensive approach ensures high accuracy, consistency, and reliability, making it particularly suitable for regional-scale studies.

The pollution gases including (CO, O_3, NO_2, SO_2) were acquired from the level 2 data products of tropospheric monitoring instrument (TROPOMI) onboard the Sentinel-5 Precursor satellite. The spatial resolution is 7 km × 3.5 km, which enables detailed monitoring of urban-scale pollution patterns, capturing localized emissions. The time resolution is 1 day, providing sufficient frequency to track diurnal and day-to-day variations in pollution levels.

The boxplots and bivariate polar plots were performed using hourly averaged CO_2 concentration and wind field data. The latter were obtained from the 'openair' package of the R software (Carslaw and Ropkins, 2012; Carslaw and Beevers, 2013).

The 72 h forward trajectories were simulated by the hybrid single-particle Lagrangian integrated trajectory) (HYSPLIT) model to analyze the possible impact range of industrial carbon emissions (Stein et al., 2015; Duc et al., 2016). The meteorology data imported to the model during the study period were obtained from the National Oceanic and Atmospheric Administration (ftp://arlftp.arlhq.noaa.gov/pub/archives/gdas1). The start time was determined based on the time corresponding to the highest daily average CO_2 concentration in the two industrial parks during the observation period.

The potential source contribution function (PSCF) and concentration weighted trajectory (CWT) methods were used to further analyze the potential impact areas of emission sources (Begum et al., 2005; Hsu et al., 2003). The details of the two models are described in **Appendix A supplementary data**.

3. Results and discussion

3.1. CO_2 emission characteristics of different industrial parks

High emissions during peak production hours can cause localized spikes in CO_2 levels, while periods of low industrial activity may lead to temporary reductions in concentrations. Furthermore, the dispersion and accumulation of these emissions are modulated by meteorological conditions, such as wind speed and atmospheric stability. Consequently, the transport and mixing of CO_2 in the atmosphere vary, resulting in different spatial distribution patterns of carbon emissions around industrial parks. Figs. 3 and 4 show the typical range-corrected backscatter signal (PR^2), CO_2 concentration, and radial wind speed obtained by scanning two DIALs in Pucheng and Nanping industrial parks at different times to characterize the trajectories of emissions. The horizontal wind speed and direction were represented by feather symbols and overlaid on polar coordinates. The blank area of Pucheng industrial park was caused by the DIAL signal being blocked by the mountain, while the absence of radial data in Nanping industrial park was due to obstruction from the chimney, which acted as a hard target in that direction.

In Fig. 3**a1-a6**, PR^2 results clearly illustrated the distinct distribution characteristics of pollutants in Pucheng industrial park on 23 August 2024. CO_2 concentration patterns shown in Fig. 3**b1-b6** followed a similar distribution trend. During the daytime, relatively low horizontal wind speeds and heterogeneous wind directions limited horizontal diffusion, causing pollutants to accumulate locally within the scanning range. Meanwhile, the predominantly positive radial wind speeds shown in Fig. 3**c1-c4** further restricted horizontal dispersion. Increased industrial activities during daylight hours led to the formation of larger areas with higher CO_2 concentrations. Additionally, daytime photosynthesis induced a characteristic temporal pattern in CO_2 concentrations. In low-concentration areas near the DIAL, CO_2 gradually decreased during the day and increased again at night. In contrast, nighttime conditions exhibited different dynamic processes. The horizontal wind speeds increased compared to the daytime, which enhanced the dispersion of pollutants and CO_2. Fig. 3**c5 and c6** shows that radial wind speeds predominantly became negative, facilitating the radial transport of CO_2 away from the DIAL. Additionally, reduced industrial production at night led to smaller high-concentration areas. A detailed analysis of temporal variations revealed that, at 21:17, both pollutants and CO_2 were transported southeastward under northwest winds. By 23:00, a shift in wind direction to the northeast redirected the transport southwestward.

Fig. 4**a1-a6 and b1-b6** illustrate a strong consistency in the distribution of PR^2 and CO_2 concentrations in Nanping industrial park on 25 September 2024, with horizontal wind speeds generally remaining low during the day and increasing at night. Notably, the diffusion direction of both pollutants and CO_2 aligned with the horizontal wind direction. Furthermore, emissions in Nanping industrial park displayed significant temporal variability and were primarily concentrated near the DIAL. In the morning, PR^2 results in Fig. 4**a1 and a2** show significant enhance-

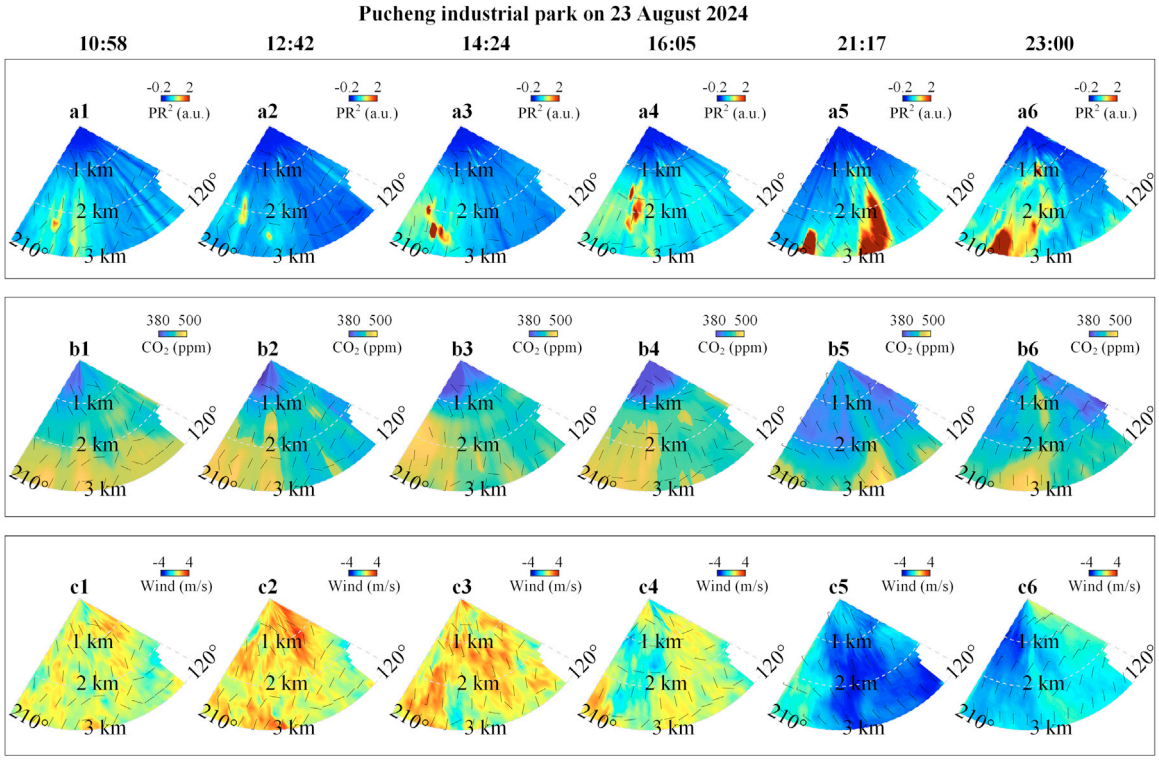

Fig. 3 – Typical spatial distribution characteristics of (a1)-(a6) PR^2, (b1)-(b6) CO_2 concentration, and (c1)-(c6) radial wind speed in Pucheng industrial park on 23 August 2024.

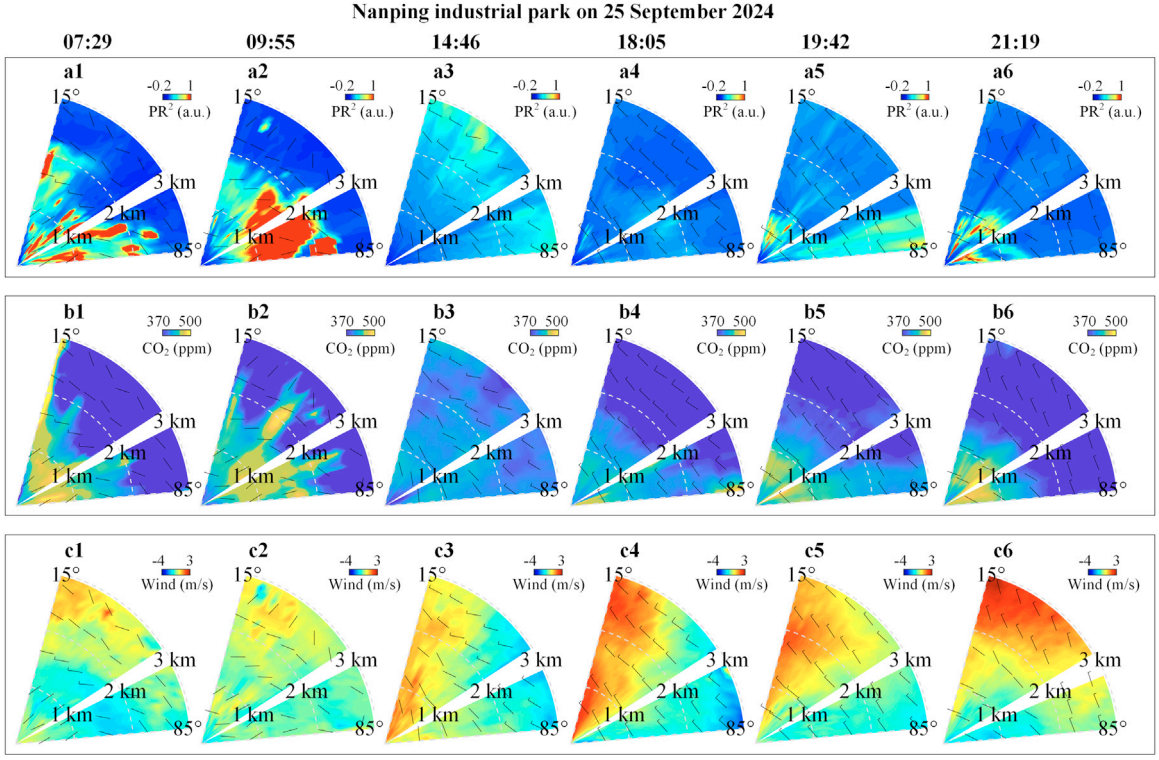

Fig. 4 – Typical spatial distribution characteristics of (a1)-(a6) PR^2, (b1)-(b6) CO_2 concentration, and (c1)-(c6) radial wind speed in Nanping industrial park on 25 September 2024.

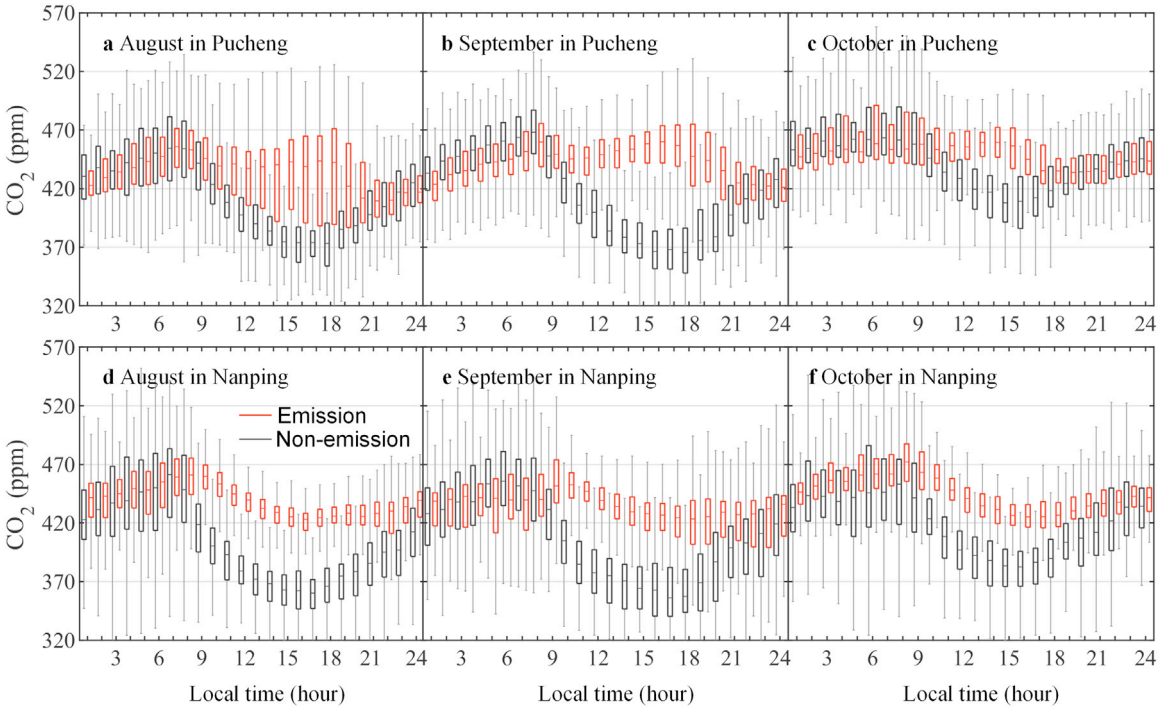

Fig. 5 – Boxplots of hourly averaged CO_2 concentration against local time from 1 August 2024 and 31 October 2024 at (a)-(c) Pucheng industrial park and (d)-(f) Nanping industrial park. The red and black boxes represent the CO_2 concentrations from emission and non-emission areas, respectively. The top, middle, and bottom horizontal lines of the box represent the 75th percentile, median, and 25th percentile, respectively. The whiskers represent the minimum and maximum values.

ment within a 2 km radius, likely resulting from a combination of factory emissions and morning fog formation. During this period, CO_2 concentrations also remained relatively high, reflecting the gradual accumulation of CO_2 during nighttime hours. In the afternoon (Fig. 4**a3, a4 and b3, b4**), a decrease in pollutants and CO_2 was observed, attributed to the combined effects of continuous emissions from industrial parks and partial absorption of CO_2 during daytime photosynthesis. As night falls (Fig. 4**a5, a6 and b5, b6**), the weakening of photosynthetic activity allowed emissions to dominate, leading to the gradual accumulation of both pollutants and CO_2 concentrations over time.

The comparison of Pucheng and Nanping industrial parks revealed both similarities and differences in pollutant and CO_2 distribution patterns. Specifically, the distribution trends between the PR^2 and CO_2 concentrations exhibited good consistency in both industrial parks under the influence of wind fields. However, Pucheng industrial park is mainly composed of synthetic leather factories and is located along a north-south axis within mountainous terrain, displaying larger daytime high-CO_2 regions due to intense industrial activity and limited horizontal diffusion. In contrast, Nanping industrial park is characterized by the chemical plant in an enclosed basin, showing more localized emissions near the DIAL with greater temporal variability and stronger influences from local conditions. These differences highlighted how distinct geographical settings, industrial compositions, and meteorological conditions shape each industrial park's unique emission and dispersion dynamics.

3.2. Diurnal variation of CO_2 concentration

Fig. 5 shows the mean diurnal cycles of atmospheric CO_2 variations at Pucheng and Nanping industrial parks by monthly averaging data from 1 August 2024 to 31 October 2024. During this period, CO_2 concentrations generally remained low across the year (Benhelal et al., 2013; Dass et al., 2024). The non-emission areas in both Pucheng and Nanping industrial parks were selected from mountainous regions adjacent to the factories, with similar land areas. Specifically, the non-emission area of the former was located within a distance of 1.8–3 km and an azimuth range of 167°–181°, while that of the latter was within a distance of 1.08–2.28 km and an azimuth range of 15°–35°. Besides, the emission areas were respectively taken in the areas of synthetic leather factories and the chemical plant shown in Fig. 1**b and c**.

Generally, the atmospheric CO_2 concentration exhibits distinct day-night variations, mainly influenced by plant photosynthesis, respiration and meteorological factors (Duan et al., 2021). Despite substantial differences in the physical settings of Pucheng and Nanping industrial parks, both industrial parks exhibited similar mean diurnal CO_2 patterns in non-emission areas, with average concentrations for the three months of 422.4 ppm and 408.7 ppm, respectively. The highest daily CO_2 concentration occurred at 8:00, while the lowest shifted progressively earlier throughout the months, from around 18:00 in August and September to around 16:00 in October. This pattern reflected the diurnal variability of CO_2 sources and sinks as well as boundary layer height (Briber et al., 2013). Overall, CO_2 concentrations were relatively high in October, and the difference between daytime and nighttime concentrations decreased compared to August and September. It is noteworthy that the daytime decrease in CO_2 concentration at Pucheng industrial park was less pronounced than at Nanping industrial park, indicating that the concentration in the non-emission area of Nanping industrial park was less influenced by industrial emissions during the day, and more affected by natural photosynthesis.

The diurnal variation of CO_2 concentrations from emission sources in Pucheng industrial park differed from that in non-emission areas with three-month average of 442.1 ppm, showing opposite trends during the day (Fig. 5**a-c**). This was attributed to the larger factory area in Pucheng industrial park, which emitted more CO_2 than was absorbed by plant photosynthesis. Between 12:00 and 17:00 in August, the CO_2 concentration from emission area at Pucheng industrial park exhibited significant fluctuations, indicating instability in the emitted CO_2 concentrations (Fig. 5**a**). In September, the difference in CO_2 concentration between emission and non-emission areas became more obvious during the day (Fig. 5**b**). In October, the difference decreased due to the

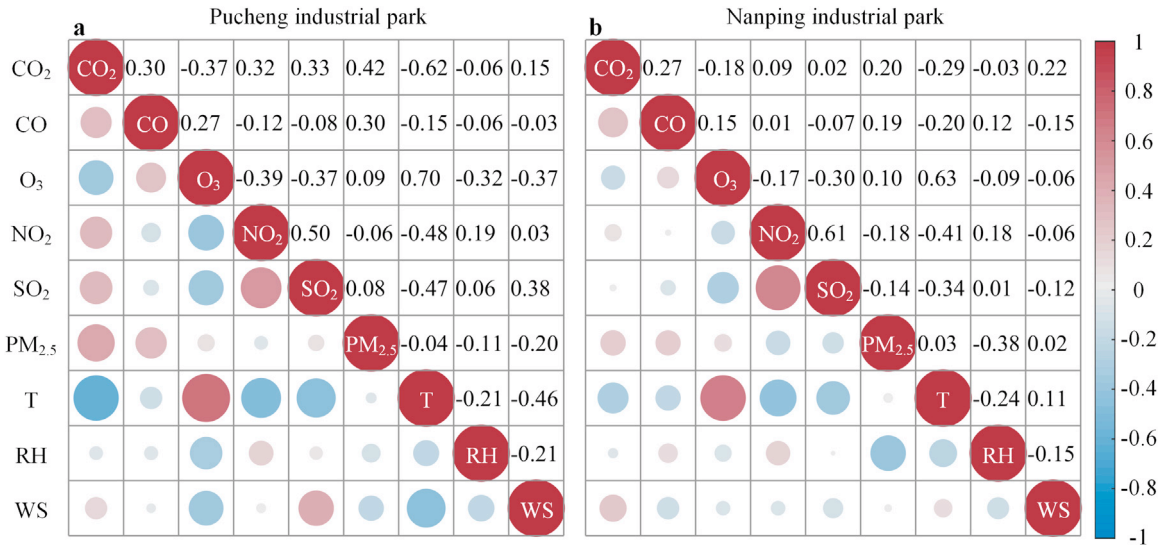

Fig. 6 – Correlations among the CO_2 from emission source and the air pollution components including CO, O_3, NO_2, SO_2 and $PM_{2.5}$, as well as the meteorological variables including air temperature (T), relative humidity (RH) and wind speed (WS). (a) Pucheng industrial park and (b) Nanping industrial park.

increase in non-emission atmospheric CO_2 concentration (Fig. 5**c**). At Nanping industrial park, the variations of emission source over the past three months remained relatively stable compared to those in Pucheng industrial park with an average of 433.5 ppm. Besides, the CO_2 concentration from emission sources showed a similar diurnal pattern to the non-emission areas, but with a smaller decrease during the day. This was the result of the combined effects of daytime plant photosynthesis and CO_2 emissions from factories. Nonetheless, the concentration variation characteristics of the two industrial parks need to be further analyzed in combination with local meteorological conditions.

3.3. The relationships between CO_2 and other atmospheric pollutants

The formation of air pollution is closely associated with the combined effects of human activities and meteorological factors. Human activities directly affect air quality through the emission of greenhouse gases and pollutants, while meteorological factors indirectly affect air quality by affecting the diffusion, accumulation, and transformation of pollutants. Industrial emissions interact with meteorological factors such as temperature, humidity, and wind speed, forming distinct air pollution patterns. Meanwhile, the emissions of various gases and particles from industrial parks into the atmosphere affect local and even larger-scale atmospheric composition and chemical reactions. The emission sources of different types of factories are diverse, thus resulting in different impacts on the atmosphere.

Fig. 6 shows the correlation between CO_2 from emission sources and gaseous pollutants (CO, O_3, NO_2, SO_2, $PM_{2.5}$) as well as meteorological parameters (air temperature, relative humidity, wind speed) in two industrial parks in Nanping City using Pearson correlation coefficient analysis. The industrial activities in both industrial parks not only contributed to atmospheric CO_2 but also released other pollutants that affect air quality. In Pucheng industrial park, CO_2 exhibited a significant positive correlation with CO, NO_2, SO_2, and $PM_{2.5}$, with correlation coefficients of 0.30, 0.32, 0.33, and 0.42, respectively. These correlations were attributed to emissions from centrally located synthetic leather factories where the burning of fossil fuels such as natural gas and coal releases substantial amounts of CO_2, NO_x (NO and NO_2), and SO_2 during heating and treatment processes (Juliadita et al., 2022). In contrast, Nanping industrial park showed weaker correlations between CO_2 and pollutants such as NO_2 and SO_2. However, CO_2 demonstrated a moderate positive correlation with CO and $PM_{2.5}$ with correlation coefficients of 0.27 and 0.20, respectively. In the chemical plant located in Nanping industrial park, NO_2 mainly originated from high-temperature combustion processes, which differed from the generation mechanism of CO_2 and CO. Additionally, the positive correlation between NO_2 and SO_2 in Nanping industrial park indirectly suggested that both pollutants were produced simultaneously, which may also include external transmission when originating from local emissions. The correlations between O_3 and CO_2 in both Nanping and Pucheng industrial parks were negative with correlation coefficients of −0.37 and −0.18. Besides, O_3 was negatively correlated with both NO_2 and SO_2, indicating that both industrial parks were VOC-sensitive regions. In the VOC-limited regime, an increase in VOCs leads to increased O_3 with a weak or even negative sensitivity to NO_x concentration (Fu et al., 2019). The stronger positive correlation between NO_2 and CO_2 in Pucheng industrial park likely exacerbated the negative relationship between CO_2 and O_3 compared to Nanping industrial park.

Temperature was a key meteorological factor influencing the behavior of most pollutant gases during the observation period. High temperatures were often accompanied by strong convective activity and enhanced atmospheric diffusion, which facilitated the dispersion and dilution of atmospheric gases and reduced gas local concentrations (Cichowicz et al., 2017; Zhang et al., 2015; Kayes et al., 2019). Elevated temperatures stimulated photosynthesis in plants, further decreasing local CO_2 concentration. Additionally, high temperatures accelerated the rate of photochemical reactions, leading to the rapid conversion of NO_2 into O_3 and other compounds. Consequently, the temperatures in both industrial parks showed negative correlations with CO_2, CO and NO_2, while presenting a strong positive correlation with O_3. The correlations between CO_2 and relative humidity were weak in both industrial parks, suggesting minimal direct interaction between humidity and CO_2. Wind speed generally showed positive correlations with CO_2, with correlation coefficients of 0.15 and 0.22 in Pucheng and Nanping industrial parks, respectively. Besides, SO_2 also showed a positive correlation with wind speed with a correlation coefficient of 0.38 in Pucheng industrial park, whereas the correlation was negative in Nanping industrial park. This suggested that high wind speeds in Pucheng industrial park transported air masses rich in CO_2-SO_2 from the upwind source to the monitoring area, resulting in a local increase in concentration, while the upwind air masses in Nanping industrial park mainly contained CO_2. Such phenomena were more likely in areas with strong nearby emission sources. Further research was needed to fully understand the mechanisms driving the relationship between wind speed and CO_2 concentrations.

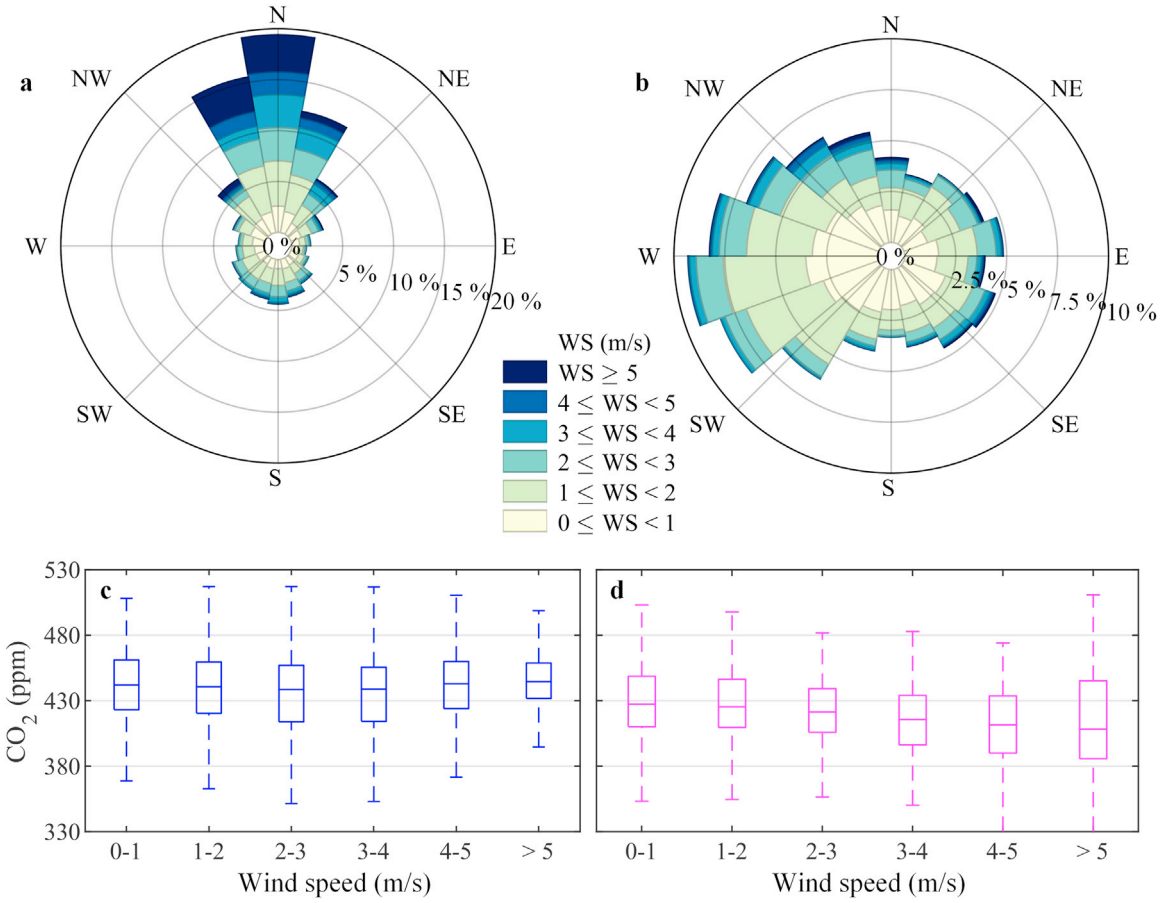

Fig. 7 – Wind rose plot from 1 August 2024 and 31 October 2024 in (a) Pucheng industrial park and (b) Nanping industrial park. Boxplots of hourly averaged CO_2 concentration against wind speed in (c) Pucheng industrial park and (d) Nanping industrial park.

3.4. Impact of local wind field on CO_2

Wind speed and direction are critical factors affecting the dilution and dispersion of atmospheric components (Ishii et al., 2010; Wang et al., 2017; Wanninkhof and Triñanes, 2017). Fig. 7**a** and **b** show the wind rose plot during the observation period at Pucheng and Nanping industrial parks, respectively, which displayed the wind direction characteristics and wind speed distribution in the study areas. During the observation period, the Pucheng industrial park experienced predominantly northward winds. Wind speed variation in this area was more pronounced, with a higher proportion of wind speeds exceeding 5 m/s. Comparatively, the wind directions at Nanping industrial park were more variable, with westerly winds being the most frequent. The wind speeds were generally lower, with most measurements below 2 m/s. Notably, the presence of several scattered factories (building materials factories) to the north of Pucheng industrial park and a cement plant to the west of Nanping industrial park likely influenced local CO_2 concentrations. Emissions from these facilities, when carried by the prevailing north or west winds, could contribute to localized increases in pollutant and gas concentrations in the surrounding areas.

Typically, CO_2 in the atmosphere is rapidly diluted and diffused at higher wind speeds, leading to a decrease in its local concentration. On the contrary, the diffusion ability of CO_2 in the air weakens when the wind speed is low, which is prone to accumulate in local areas and leads to an increase in concentration. However, the influence of wind speed is also affected by factors such as terrain, meteorological conditions, and emission source intensity. Fig. 7**c** and **d** present the boxplots of CO_2 concentrations as a function of wind speed increment in Pucheng and Nanping industrial parks during the observation period. Under calm weather conditions with wind speeds below 2 m/s, CO_2 emitted from local sources accumulated, leading to higher concentrations. As wind speed increased from 2 m/s to 4 m/s, CO_2 concentrations generally decreased due to dilution effects. However, as mentioned earlier, strong winds enhance horizontal diffusion, they can also carry pollutants from upwind areas, leading to high CO_2 loadings (Gupta et al., 2017; Duan et al., 2021). This effect was particularly evident in Pucheng industrial park, where CO_2 concentrations plateaued and slightly increased when wind speeds exceeded 4 m/s (Fig. 7**c**). This is probably due to the terrain of the industrial park, which is distributed along the north-south axis in the mountainous area, influencing local wind patterns and facilitating the regional transport of gases and pollutants. Therefore, regional transportation also played an important role in CO_2 concentration in this industrial park. Potential sources may include both industrial emissions from the scattered factories in the northern and transboundary atmospheric transport of pollutants from adjacent northern areas. In contrast, the CO_2 concentrations in Nanping industrial park consistently decreased with the increased wind speed (Fig. 7**d**). The reason is that the enclosed basin topography, characterized by surrounding mountainous terrain, likely restricted the influence of regional transport by acting as a natural barrier to airflow from upwind areas. Consequently, the contribution of transported CO_2 from external sources in this industrial park was less pronounced, and local emissions were the primary factor affecting CO_2 levels.

The bivariate polar plot provides an efficient graphical method for detecting sources and understanding the characteristics by combining wind speed and direction together with the CO_2 concentrations. Figs. 8 and 9 display the bivariate polar plots for CO_2 concentrations at the Pucheng and Nanping industrial parks during the observation pe-

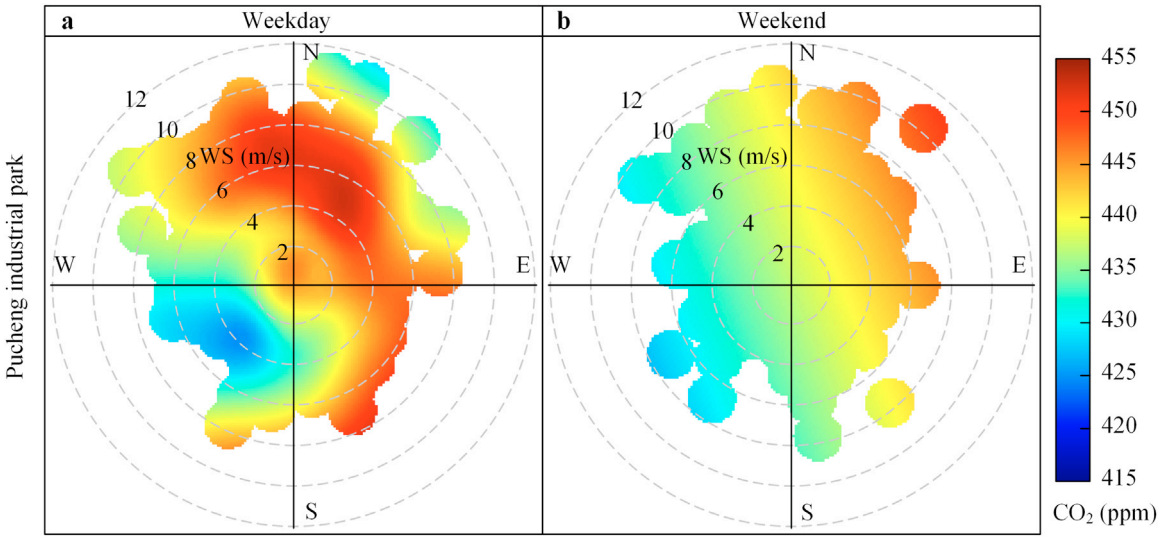

Fig. 8 – Winds-dependent variations of hourly averaged CO_2 concentrations from 1 August 2024 and 31 October 2024 at Pucheng industrial park. (a) Weekday and (b) Weekend.

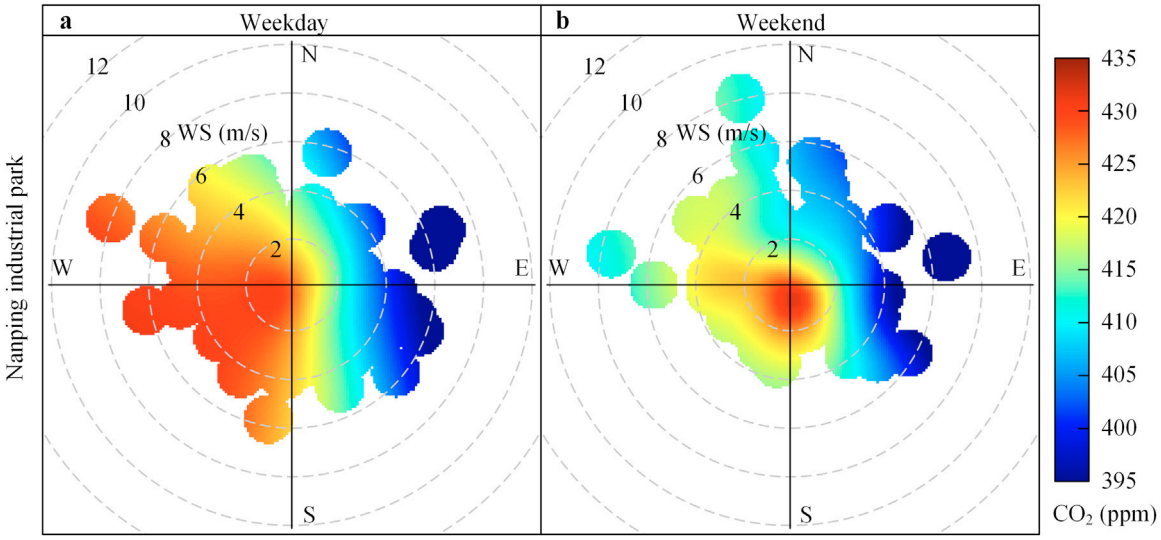

Fig. 9 – Winds-dependent variations of hourly averaged CO_2 concentrations from 1 August 2024 and 31 October 2024 at Nanping industrial park. (a) Weekday and (b) Weekend.

riod. Researches show that CO_2 varies between weekdays (Monday–Friday) and weekends (Saturday–Sunday) due to differences in human activity patterns, traffic volumes, and industrial production schedules (Nasrallah et al., 2003; Weissert et al., 2015; Wang et al., 2022). The phenomenon is known as the weekday-weekend effect.

During the observation period, Pucheng industrial park exhibited obvious variations in CO_2 concentrations between weekdays and weekends in relation to wind speed and direction. On weekdays, CO_2 concentrations were higher, exceeding 450 ppm under stronger winds (> 5 m/s) from the north, while lower concentrations (< 430 ppm) were observed under weaker winds (< 5 m/s) from the southwest (Fig. 8**a**). On weekends, the overall CO_2 concentrations were lower, with higher concentrations (> 440 ppm) associated with winds from the northeast and lower concentrations (< 430 ppm) from the southwest and northwest (Fig. 8**b**). This can be attributed to the fact that both the scattered factories located in the north of the observation point and the synthetic leather factories reduced emissions on weekends. The patterns highlighted the combined effects of both local and regional sources on elevated CO_2 levels in Pucheng industrial park.

In Nanping industrial park, the weekday-weekend effect on CO_2 concentrations with respect to wind speed and direction was also observed. Since the eastern side of the scanning area is predominantly forested, the eastward winds were associated with lower CO_2 concentrations, with concentrations decreasing as wind speed increased. On weekdays, high CO_2 concentrations (> 430 ppm) occurred in the southwest direction, with higher concentrations compared to other directions. Both high and low wind speeds in these directions corresponded to higher CO_2 levels (Fig. 9**a**). On weekends, CO_2 levels remained relatively high, with concentrations exceeding 430 ppm under lower wind speeds (< 2 m/s) (Fig. 9**b**). This indicated that carbon emissions in the region persisted, albeit at reduced levels compared to weekdays. Besides, the patterns also suggested that the increase in CO_2 concentrations in Nanping industrial park was primarily driven by local emissions from the chemical plant and the cement plant to the west of the DIAL, along with westerly wind transport on weekdays (Benhelal et al., 2013; Shen et al., 2015). During weekends, local emissions from the chemical plant were the primary contributor to elevated CO_2 levels.

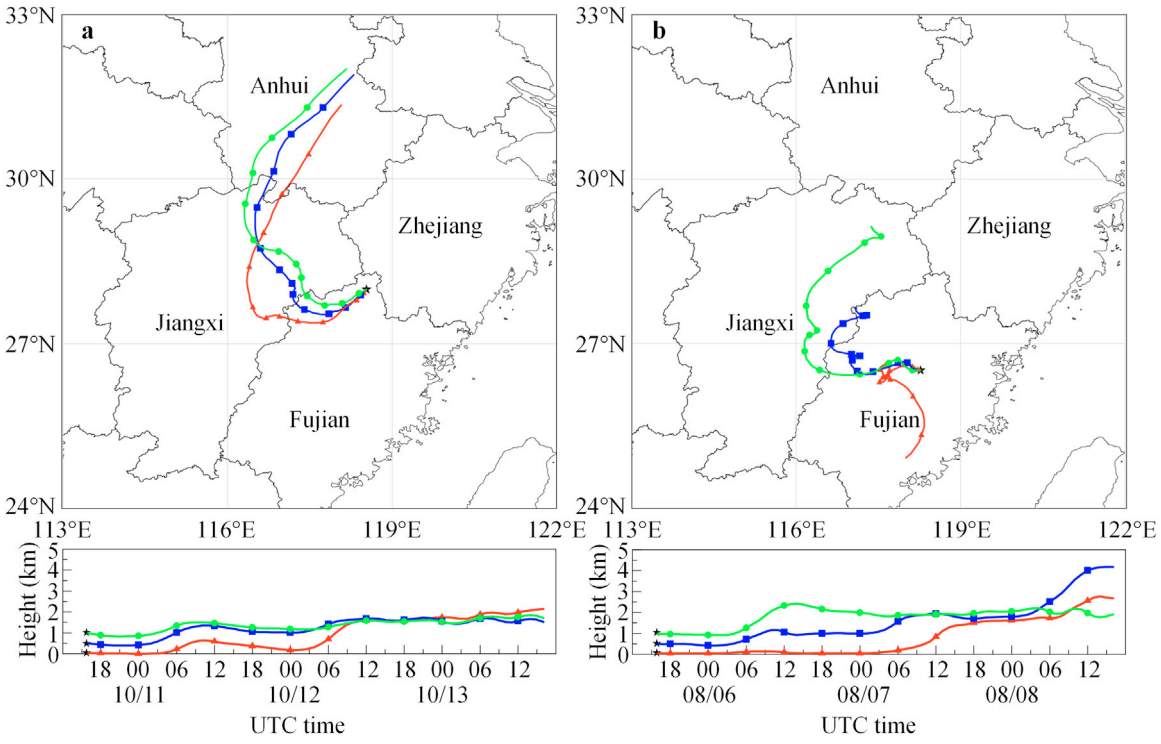

Fig. 10 – Simulation results of forward trajectories at 50 m, 500 m and 1000 m above the (a) Pucheng industrial park starting at 16:00 UTC on 10 October 2024 (00:00 local time on 11 October 2024) and (b) Nanping industrial park starting at 16:00 UTC on 5 August 2024 (00:00 local time on 6 August 2024).

3.5. Possible impact areas of emission sources

Regional air mass transport played a critical role in shaping atmospheric CO_2 concentrations. The forward trajectory analysis based on HYSPLIT is a method used to predict the future path of air mass from a known starting point, helping to estimate the dispersion trends of pollutants (McGowan and Clark, 2008). The analysis above indicated that the highest daily average emission concentrations, with values of 486.8 and 461.1 ppm, were observed in Pucheng and Nanping industrial parks on 11 October 2024 and 6 August 2024, respectively.

Fig. 10**a** shows the forward trajectory of Pucheng industrial park at the height of 50 m, 500 m and 1000 m above the model ground level, starting at 16:00 UTC on 10 October 2024 and ending at 16:00 UTC on 13 October 2024. Starting the simulation at 16:00 UTC allowed to trace the dispersion of pollutants during and after the peak emission event. At the height of 50 m, the air mass initially moved southwest from Pucheng County, passing through Shaowu City before continuing westward. It arrived in the eastern part of Jiangxi Province around 21:00 UTC on 11 October (5:00 local time on 12 October) and then began moving northeast. After passing through Fuzhou City in Jiangxi Province, the air mass arrived in southern Anhui Province around 06:00 UTC on October 13 (14:00 local time on October 13) and then crossed over Chizhou City and Tongling City, eventually reaching an altitude of 2 km above Wuhu City. At the heights of 500 m and 1000 m, the trajectories showed similar patterns. The air mass moved southwest, reaching the vicinity of the Mount Wuyi Mountains around 06:00 UTC (14:00 local time on October 11). From there, the air mass moved northwest, passing Yingtan City and Shangrao City in Jiangxi Province, crossing 1.5 km above Poyang Lake and continuing to move northeast. After that the air mass arrived in Anhui Province at about 23:00 UTC (7:00 local time on 14 October), and finally reached 1.5 km above Ma'anshan City and Chuzhou City after passing Anqing City in Anhui Province. Therefore, during the observation period, the CO_2 emissions from Pucheng industrial park primarily affected the northern part of Fujian Province, the northeastern part of Jiangxi Province, and some areas in the southern part of Anhui Province.

Fig. 10**b** shows the forward trajectory of Nanping industrial park at the height of 50 m, 500 m and 1000 m above the model ground level, starting at 16:00 UTC on 5 August 2024 and ending at 16:00 UTC on 8 August 2024. The air mass at a height of 50 m moved northwest, passing Yanping District before turning southwest and reaching Sanming City in Fujian Province. After staying there for two days, the air mass turned southeast at 24:00 UTC on 8 August (8:00 local time on 9 August) and finally ascended to an altitude of 2.7 km over Anxi County in Quanzhou City. The transmission trajectory of the air mass at a height of 500 m before 18:00 UTC on 6 August (2:00 local time on 7 August) was similar to that of the air mass at a height of 1000 m, both moving westward from the starting point and reaching the territory of Sanming City. Then, the air mass at a height of 500 m turned northwest and reached the border of Jiangxi Province at 18:00 UTC on 7 August (2:00 local time on 8 August). It then turned northeast and finally returned to Guangze County in Fujian Province. Meanwhile, the air mass at a height of 1000 m continued westward, reaching the eastern part of Jiangxi Province by 14:00 UTC on 6 August, then went north through Fuzhou City in Jiangxi Province and finally reached a height of 1.5 km in Jingdezhen City in northeastern Jiangxi Province. Therefore, during the observation period, the CO_2 emissions from Nanping industrial park mainly affected the southern and western parts of Fujian Province, as well as the northeastern part of Jiangxi Province.

To comprehensively investigate the potential regional impacts of emission sources, a detailed statistical analysis utilizing 72-hour forward trajectories combined with PSCF and CWT methods was conducted (Details in Appendix A supplementary data). The analysis specifically focused on the three-month observation period, with trajectory initialization set at 50 m above the model ground level to capture near-surface transport patterns (Appendix A Figs. S1-S6). During the observation period, the distribution of PSCF and CWT revealed distinct regional impacts from the two industrial parks. Specifically, Pucheng industrial park showed longer transmission paths and higher CO_2 concentrations, while Nanping industrial park demonstrated more localized and southward-reaching trajectories. In general, the emissions from the

two industrial parks during the three months of observations primarily impacted regions in southeastern China, particularly Fujian and its adjacent provinces, including eastern Jiangxi, eastern Guangdong, and parts of southern Zhejiang.

4. Conclusions

In this study, two coherent DIALs were employed to remotely sense the atmospheric CO_2 concentration and wind field in two industrial parks located at the north and south ends of Nanping City from August to October 2024. The study provided valuable data to assess the impacts of different industrial emission sources on atmospheric CO_2 levels.

The spatial distribution characteristics of CO_2 emissions were clarified within a radius of 3 km and azimuth angles of 120°–210° and 15°–85° for Pucheng and Nanping industrial parks, respectively. By analyzing the carbon emission distribution at different times, the approximate trajectory of its movement under the influence of the wind fields has been determined. Besides, both DIALs successfully identified CO_2 concentration differences between the factory areas and the surrounding areas under the interplay of wind field and emission sources. Daily variation statistics from emission and non-emission areas showed that the CO_2 concentrations in emission areas at Pucheng industrial park were higher and more variable than those at Nanping industrial park, indicating that Pucheng industrial park was more impacted by local emissions. The CO_2 concentrations in non-emission areas followed a regular diurnal pattern, with concentrations gradually increasing over August to October. The average values in non-emission areas for the past three months of 422.4 ppm and 408.7 ppm of Pucheng and industrial parks, respectively. Beyond CO_2, emissions from both industrial parks contributed to other pollutants affecting air quality. Correlation analysis revealed that the synthetic leather factories in Pucheng industrial park were also an important source of SO_2 and NO_x compared to the chemical plant in Nanping industrial park. Based on the analysis of meteorological conditions in both locations, Pucheng industrial park was influenced mainly by the stronger north wind, which caused slight CO_2 increases under wind speeds above 4 m/s. It indicated that regional transport accelerated the diffusion of CO_2 under high wind speed conditions. Nanping industrial park was primarily affected by the west wind. It showed decreased CO_2 concentrations with increasing wind speed, indicating localized emissions as the dominant source. In addition, distinct weekday-weekend emission patterns were observed in both industrial parks, with a decrease in weekend emissions compared to weekdays. Forward trajectory simulations during high-emission periods revealed that emissions from Pucheng industrial mainly affected the southern part of Fujian, the northeastern part of Jiangxi, and the southern part of Anhui Provinces, while Nanping emissions were primarily confined to central and western parts of Fujian and part of Jiangxi Provinces. During the three-month observation period, the distribution of PSCF and CWT revealed that emissions from the two industrial parks primarily influenced Fujian and its adjacent provinces including eastern Jiangxi, eastern Guangdong, and parts of southern Zhejiang.

In summary, carbon emission sources at different locations exhibit varying impacts on the spatiotemporal distribution of atmospheric CO_2 concentration. Although the limited DIAL measurements may not represent the entire atmosphere, they provide critical information about industrial emissions in mountainous areas and the dynamics of local CO_2 sources-sink, as well as important insights into the interaction between human emissions and natural carbon transport.

Declaration of competing interest

The authors declare that they have no known competing financial interests or personal relationships that could have appeared to influence the work reported in this paper.

CRediT authorship contribution statement

Saifen Yu: Writing – review & editing, Writing – original draft, Validation, Software, Methodology, Investigation, Funding acquisition, Data curation, Conceptualization. **DaiHao Yu:** Writing – review & editing, Validation, Investigation, Data curation. **Qiuwei xia:** Writing – review & editing, Validation, Data curation. **Yixiang Chen:** Writing – review & editing, Data curation. **Zhen Zhang:** Writing – review & editing, Methodology, Funding acquisition, Data curation, Conceptualization. **Haiyun Xia:** Writing – review & editing, Conceptualization.

Acknowledgments

This work was supported by the National Natural Science Foundation of China (Nos. 42305147 and 42405138) and the Natural Science Foundation of Jiangsu Province (No. BK20230428).

Appendix A Supplementary data

Supplementary material associated with this article can be found in the online version at doi:10.1016/j.jes.2025.03.046.

References

Andres, R.J., Boden, T.A., Bréon, F.M., Ciais, P., Davis, S., Erickson, D., et al., 2012. A synthesis of carbon dioxide emissions from fossil-fuel combustion. Biogeosciences 9 (5), 1845–1871.
Begum, B.A., Kim, E., Jeong, C.H., Lee, D.W., Hopke, P.K., 2005. Evaluation of the potential source contribution function using the 2002 Quebec forest fire episode. Atmos. Environ. 39 (20), 3719–3724.
Benhelal, E., Zahedi, G., Shamsaei, E., Bahadori, A., 2013. Global strategies and potentials to curb CO_2 emissions in cement industry. J. Clean. Prod. 51, 142–161.
Briber, B.M., Hutyra, L.R., Dunn, A.L., Raciti, S.M., Munger, J.W., 2013. Variations in atmospheric CO_2 mixing ratios across a Boston, MA urban to rural gradient. Land 2 (3), 304–327.
Carslaw, D.C., Ropkins, K., 2012. Openair—An R package for air quality data analysis. Environ. Model. Softw. 27, 52–61.
Carslaw, D.C., Beevers, S.D., 2013. Characterising and understanding emission sources using bivariate polar plots and k-means clustering. Environ. Model. Softw. 40, 325–329.
Chen, J., Cao, X., Peng, S., Ren, H., 2017. Analysis and applications of GlobeLand30: a review. ISPRS Int. J. Geo Inf. 6 (8), 230.
Cheng, S., Zhou, L., Tans, P.P., An, X., Liu, Y., 2018. Comparison of atmospheric CO_2 mole fractions and source–sink characteristics at four WMO/GAW stations in China. Atmos. Environ. 180, 216–225.
Chowdhury, Z.U.M., Ahmed, T., Hashem, M.A., 2017. Materials and energy flow in the life cycle of leather: a case study of Bangladesh. Mater. Technique-FR 105 (5–6), 502.
Cichowicz, R., Wielgosiński, G., Fetter, W., 2017. Dispersion of atmospheric air pollution in summer and winter season. Environ. Monit. Assess. 189, 1–10.
Dass, A., Mishra, A.K., de Araújo Santos, G.A., Ranjan, R.K., 2024. Spatio-temporal variation of atmospheric CO_2 and its association with anthropogenic, vegetation, and climate indices over the state of Bihar, India. Environ. Adv. 16, 100513.
Duan, Z., Yang, Y., Wang, L., Liu, C., Fan, S., Chen, C., et al., 2021. Temporal characteristics of carbon dioxide and ozone over a rural-cropland area in the Yangtze River Delta of eastern China. Sci. Total Environ. 757, 143750.
Duc, H.N., Bang, H.Q., Quang, N.X., 2016. Modelling and prediction of air pollutant transport during the 2014 biomass burning and forest fires in peninsular Southeast Asia. Environ. Monit. Assess. 188, 1–23.
Fang, S.X., Zhou, L.X., Tans, P.P., Ciais, P., Steinbacher, M., Xu, L., et al., 2014. In situ measurement of atmospheric CO_2 at the four WMO/GAW stations in China. Atmos. Chem. Phys. 14 (5), 2541–2554.
Friedlingstein, P., O'sullivan, M., Jones, M.W., Andrew, R.M., Gregor, L., Hauck, J., et al., 2022. Global carbon budget 2022. Earth Syst. Sci. Data 14 (11), 4811–4900.
Friedlingstein, P., O'Sullivan, M., Jones, M.W., Andrew, R.M., Bakker, D.C.E., Hauck, J., et al., 2023. Global carbon budget 2023. Earth Syst. Sci. Data 15, 5301–5369.
Fu, Y., Liao, H., Yang, Y., 2019. Interannual and decadal changes in tropospheric ozone in China and the associated chemistry-climate interactions: a review. Adv. Atmos. Sci. 36 (9), 975–993.
Gibert, F., Edouart, D., Cénac, C., Le Mounier, F., Dumas, A., 2015. 2-μm Ho emitter-based coherent DIAL for CO_2 profiling in the atmosphere. Opt. Lett. 40 (13), 3093–3096.
Gregg, J.S., Andres, R.J., Marland, G., 2008. China: emissions pattern of the world leader in CO_2 emissions from fossil fuel consumption and cement production. Geophys. Res. Lett. 35 (8), L08806.
Gupta, P., Singh, S.P., Jangid, A., Kumar, R., 2017. Characterization of black carbon in the ambient air of Agra, India: seasonal variation and meteorological influence. Adv. Atmos. Sci. 34, 1082–1094.
Henninger, S., Kuttler, W., 2010. Near surface carbon dioxide within the urban area of Essen, Germany. Phys. Chem. Earth 35 (1–2), 76–84.
Hofmann, D.J., Butler, J.H., Tans, P.P., 2009. A new look at atmospheric carbon dioxide. Atmos. Environ. 43 (12), 2084–2086.

Hsu, Y.K., Holsen, T.M., Hopke, P.K., 2003. Comparison of hybrid receptor models to locate pcb sources in chicago. Atmos. Environ. 37 (4), 545–5626.
Ishii, S., Mizutani, K., Fukuoka, H., Ishikawa, T., Philippe, B., Iwai, H., et al., 2010. Coherent 2 μm differential absorption and wind lidar with conductively cooled laser and two-axis scanning device. Appl. Opt. 49 (10), 1809–1817.
Juliadita, A.K., Hermiyanti, P., Myers, J.P., 2022. Risk analysis of NO_2 and SO_2 gas exposure for leather tannery workers industry at Magetan. Adv. Health Sci. Technol. 2 (5), 285–291.
Kayes, I., Shahriar, S.A., Hasan, K., Akhter, M., Kabir, M.M., Salam, M.A., 2019. The relationships between meteorological parameters and air pollutants in an urban environment. Glob. J. Environ. Sci. Manag. 5 (3), 265–278.
Koch, G.J., Barnes, B.W., Petros, M., Beyon, J.Y., Amzajerdian, F., Yu, J., et al., 2004. Coherent differential absorption lidar measurements of CO_2. Appl. Opt. 43 (26), 5092–5099.
Lahyani, J., Le Gouët, J., Gibert, F., Cézard, N., 2021. 2.05-μm all-fiber laser source designed for CO_2 and wind coherent lidar measurement. Appl. Opt. 60 (15), C12–C19.
Lan, X., Tans, P., Thoning, K.W., 2024. Trends in Globally-Averaged CO_2 Determined from NOAA Global Monitoring Laboratory measurements. Version 2024–10. National Oceanic and Atmospheric Administration (NOAA) Global Monitoring Laboratory.
Le Quéré, C., Raupach, M.R., Canadell, J.G., Marland, G., Bopp, L., Ciais, P., et al., 2009. Trends in the sources and sinks of carbon dioxide. Nat. Geosci. 2 (12), 831–836.
Lewicki, J.L., Bergfeld, D., Cardellini, C., Chiodini, G., Granieri, D., Varley, N., et al., 2005. Comparative soil CO_2 flux measurements and geostatistical estimation methods on Masaya volcano. Nicaragua. Bull. Volcanol. 68 (1), 76–90.
Li, S., Chen, L., Xiong, X., Tao, J., Su, L., Han, D., et al., 2012. Retrieval of the haze optical thickness in North China Plain using MODIS data. IEEE Trans. Geosci. Remote Sens. 51 (5), 2528–2540.
Lobell, D.B., Burke, M.B., Tebaldi, C., Mastrandrea, M.D., Falcon, W.P., Naylor, R.L., 2008. Prioritizing climate change adaptation needs for food security in 2030. Science 319 (5863), 607–610.
Lüthi, D., Le Floch, M., Bereiter, B., Blunier, T., Barnola, J.M., Siegenthaler, U., et al., 2008. High-resolution carbon dioxide concentration record 650,000–800,000 years before present. Nature 453 (7193), 379–382.
McGowan, H., Clark, A., 2008. Identification of dust transport pathways from Lake Eyre, Australia using Hysplit. Atmos. Environ. 42 (29), 6915–6925.
Nasrallah, H.A., Balling Jr, R.C., Madi, S.M., Al-Ansari, L., 2003. Temporal variations in atmospheric CO_2 concentrations in Kuwait City, Kuwait with comparisons to Phoenix, Arizona, USA. Env. Poll. 121 (2), 301–305.
Pan, Y., Birdsey, R.A., Fang, J., Houghton, R., Kauppi, P.E., Kurz, W.A., et al., 2011. A large and persistent carbon sink in the world's forests. Science 333 (6045), 988–993.
Prentice, I.C., Farquhar, G.D., Fasham, M.J.R., Goulden, M.L., Heimann, M., Jaramillo, V.J., et al., 2001. The carbon cycle and atmospheric carbon dioxide. In: Houghton, R.A., Ding, Y., Griggs, D. (Eds.), Climate Change 2001: The Scientific Basis. Cambridge, Cambridge University Press.
Queißer, M., Granieri, D., Burton, M., 2016. A new frontier in CO_2 flux measurements using a highly portable DIAL laser system. Sci. Rep. 6 (1), 33834.
Queißer, M., Burton, M., Kazahaya, R., 2019. Insights into geological processes with CO_2 remote sensing–A review of technology and applications. Earth Sci. Rev. 188, 389–426.
Shen, W., Cao, L., Li, Q., Zhang, W., Wang, G., Li, C., 2015. Quantifying CO_2 emissions from China's cement industry. Renew. Sustain. Energy Rev. 50, 1004–1012.
Stein, A.F., Draxler, R.R., Rolph, G.D., Stunder, B.J., Cohen, M.D., Ngan, F., 2015. NOAA's HYSPLIT atmospheric transport and dispersion modeling system. B. Am. Meteorol. So. 96 (12), 2059–2077.
Turnbull, J.C., Tans, P.P., Lehman, S.J., Baker, D., Conway, T.J., Chung, Y.S., et al., 2011. Atmospheric observations of carbon monoxide and fossil fuel CO_2 emissions from East Asia. J. Geophys. Res-Atmos. 116 (D24), D24306.
Van Oosterhout, R., Striekwold, P., Wang, M., 2024. On data-induced CO_2 emissions of vehicle automation: an overlooked emission source. Sustain. Horiz. 9, 100082.
Wang, Q., Zhao, Z., Tian, J., Zhu, C., Ni, H., Zhang, Y., et al., 2017. Seasonal transport and dry deposition of black carbon aerosol in the southeastern Tibetan plateau. Aerosol. Sci. Eng. 1, 160–168.
Wang, H., Gong, F.Y., Newman, S., Zeng, Z.C., 2022. Consistent weekly cycles of atmospheric NO_2, CO, and CO_2 in a North American megacity from ground-based, mountaintop, and satellite measurements. Atmos. Environ. 268, 118809.
Wanninkhof, R., Triñanes, J., 2017. The impact of changing wind speeds on gas transfer and its effect on global air-sea CO_2 fluxes. Global Biogeochem. Cy. 31 (6), 961–974.
Weissert, L.F., Salmond, J.A., Friedel, A., LaFave, M., Schwendenmann, L., 2015. In: Temporal and Spatial Patterns of Carbon Dioxide Mixing Ratios in a Subtropical Urban Environment During Spring, 35. Weather Clim, pp. 13–32.
Xia, L., Zhou, L., Tans, P.P., Liu, L., Zhang, G., Wang, H., Luan, T., 2015. Atmospheric CO_2 and its $\delta^{13}C$ measurements from flask sampling at Lin'an regional background station in China. Atmos. Environ. 117, 220–226.
Xia, L., Zhang, G., Liu, L., Li, B., Zhan, M., Kong, P., et al., 2020. Atmospheric CO_2 and CO at Jingdezhen station in Central China: understanding the regional transport and combustion efficiency. Atmos. Environ. 222, 117104.
Yu, S., Zhang, Z., Li, M., Xia, H., 2021a. Multi-frequency differential absorption lidar incorporating a comb-referenced scanning laser for gas spectrum analysis. Opt. Express 29 (9), 12984–12995.
Yu, S., Zhang, Z., Xia, H., Dou, X., Wu, T., Hu, Y., et al., 2021b. Photon-counting distributed free-space spectroscopy. Light-Sci. Appl. 10 (1), 212.
Yu, S., Guo, K., Li, S., Han, H., Zhang, Z., Xia, H., 2024. Three-dimensional detection of CO_2 and wind using a 1.57 μm coherent differential absorption lidar. Opt. Express 32 (12), 21134–21148.
Yuan, J., Su, L., Xia, H., Li, Y., Zhang, M., Zhen, G., et al., 2022. Microburst, windshear, gust front, and vortex detection in mega airport using a single coherent Doppler wind lidar. Remote Sens. 14 (7), 1626.
Yue, B., Yu, S., Li, M., Wei, T., Yuan, J., Zhang, Z., et al., 2022. Local-scale horizontal CO_2 flux estimation incorporating differential absorption lidar and coherent Doppler wind lidar. Remote Sens. 14 (20), 5150.
Zhang, H., Guo, W., Wang, S., Yao, Z., Lv, L., Teng, Y., et al., 2024. Insights into the spatiotemporal heterogeneity, sectoral contributions and drivers of provincial CO_2 emissions in China from 2019 to 2022. J. Environ. Sci. 155, 510–524.
Zhang, H., Wang, Y., Hu, J., Ying, Q., Hu, X.M., 2015. Relationships between meteorological parameters and criteria air pollutants in three megacities in China. Environ. Res. 140, 242–254.
Zhao, L., Fan, X., Lin, H., Hong, T., Hong, W., 2021. Impact of urbanization on the value of ecosystem services in Nanping City, China. Pol. J. Environ. Stud. 30, 965–975.